ACS Catalysis

Research Article

Cite This: ACS Catal. 2018, 8, 3076−3086

pubs.acs.org/acscatalysis

Distinguishing Active Site Identity in Sn-Beta Zeolites Using ^{31}P MAS NMR of Adsorbed Trimethylphosphine Oxide

Jennifer D. Lewis,[†] Michelle Ha,[‡] Helen Luo,[†] Alexandra Faucher,[‡,§] Vladimir K. Michaelis,*[,‡] and Yuriy Román-Leshkov*[,†]

[†]Department of Chemical Engineering, Massachusetts Institute of Technology, 77 Massachusetts Avenue, Cambridge, Massachusetts 02139, United States

[‡]Department of Chemistry, Gunning-Lemieux Chemistry Centre, University of Alberta, Edmonton, Alberta, Canada T6G 2G2

Supporting Information

ABSTRACT: The identity of the active sites of hydrophobic Lewis acid zeolites was elucidated by solid-state ^{31}P nuclear magnetic resonance (NMR) spectroscopy following adsorption of trimethylphosphine oxide (TMPO) probe molecules. The adsorption of TMPO on these materials resulted in distinct ^{31}P NMR resonances between δ_{iso} = 59.9 and 54.9 ppm that correspond to unique chemical environments of the Lewis acidic heteroatoms in the Beta zeolite framework. The ^{31}P NMR resonances were assigned to sites in Sn-Beta zeolites by correlating the variation of ^{31}P NMR spectra during TMPO titration experiments with the corresponding changes in the ^{119}Sn NMR spectra. This method allowed us to establish quantitative relationships between the assignments for each site and the catalytic activity for the glucose isomerization and aldol condensation reactions. The rate of glucose isomerization directly correlated with the combined integrated intensities of ^{31}P MAS NMR resonances at δ_{iso} = 55.8 and 54.9 ppm, which amounted to 12−33% of total Sn sites. In contrast, the integrated peak area of a different site at δ_{iso} = 58.6 ppm was shown to correlate with aldol condensation activity. The probing method used to identify and quantify distinct active sites within the framework of low-defect Lewis acid zeolites developed in this work is applicable to a wide range of microporous materials, regardless of heteroatom identity.

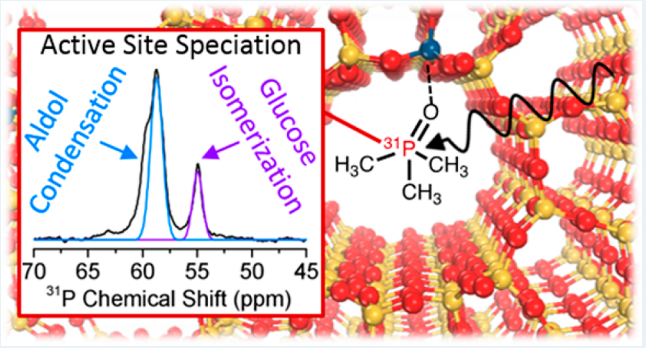

KEYWORDS: *zeolites, Lewis acid, phosphine oxides, probe molecule adsorption, Sn-Beta, titration, glucose isomerization, aldol condensation*

INTRODUCTION

Lewis acid zeolites, such as Sn- and Ti-Beta, have emerged as exceptional catalysts for the activation of oxygenated molecules and are of special interest for biomass conversion schemes. The synthesis of these materials in fluoride media produces low-defect zeolites with increased hydrothermal stability, crystallinity, and hydrophobicity.[1,2] These zeolites are capable of catalyzing a wide range of transformations, including oxidation, transfer hydrogenation, sugar isomerization, (retro)aldol, and Diels−Alder reactions.[3−11] Interest in Lewis acid zeolites has led to numerous studies investigating their catalytic properties and attempting to decipher the true origin of their unique catalytic activity. However, as evidenced by many conflicting reports in the open literature, the nature of the active sites in these materials continues to be poorly understood.[12,13]

Experimental evidence for the active site speciation in Sn-Beta and other M-Beta zeolites is difficult to obtain given the limited spectroscopic techniques available that can resolve the identity of these sites. Tin-119 magic-angle spinning nuclear magnetic resonance (MAS NMR) spectroscopy has been used to show the presence of multiple tetrahedral sites in Sn-Beta catalysts, although the assignment of these sites continues to be debated.[14] This technique is limited by the need for enriched ^{119}Sn samples due to the low natural abundance (8.6%) of the ^{119}Sn isotope and the limited metal content (up to 2 wt %) of hydrothermally synthesized Sn-Beta. Dynamic nuclear polarization (DNP) NMR[15−17] and Carr−Purcell−Meiboom−Gill (CPMG) echo train acquisition[14,18] are two methods that have allowed for analysis of Sn-containing zeolites at natural abundance. However, the former is not quantitative, and the latter is highly dependent on spin−spin nuclear relaxation (T_2) behaviors, hindering robust quantification. While powerful, MAS NMR is difficult to implement for quadrupolar nuclei with moderate to large nuclear electric quadrupole moments, such as $^{47/49}$Ti, $^{177/179}$Hf, and ^{91}Zr.

Received: October 16, 2017
Revised: February 21, 2018
Published: February 28, 2018

DOI: 10.1021/acscatal.7b03533
ACS Catal. 2018, 8, 3076−3086

Recently, progress has been made in developing Fourier transform infrared spectroscopy (FTIR) techniques that can analyze Lewis acid zeolite active sites with the assistance of probe molecules. Boronat et al. showed that two sites in Sn-Beta can be distinguished with FTIR by absorbing deuterated acetonitrile (CD_3CN),[19] and Harris et al. quantified the concentration of each of these titrated sites in various Sn-Beta samples by accurately measuring molar extinction coefficients.[20] However, this method cannot be employed for other M-Beta zeolites, including Zr- and Hf-Beta, as only one band between 2300 and 2310 cm^{-1} is distinguishable post CD_3CN adsorption.[21,22] Sushkevich et al. showed that CO adsorption at cryogenic temperatures provides more resolution for Zr-containing zeolites and used this method to assign an active site for the synthesis of butadiene from ethanol.[22,23] The calculation of unique molar extinction coefficients for each zeolite active site is complicated by the heavily convoluted FTIR bands, making comparisons between samples, especially those with different heteroatoms, very difficult.

Unlike vibrational spectroscopy, NMR spectroscopy is a direct nucleus-specific analytical method that provides both quantitative and qualitative information without the need for molar extinction coefficients. Indeed, coupling probe molecule adsorption with NMR spectroscopy is a powerful, yet relatively unexplored technique for investigating Lewis acid zeolites. Gunther et al. recently used pyridine adsorption with ^{15}N MAS NMR to determine an acidity scale for various Lewis acid zeolites.[24] This technique was used by Gounder and co-workers to distinguish two types of sites in Sn-CHA zeolites.[25] We propose that pairing phosphorus probe molecules with ^{31}P MAS NMR spectroscopy offers a powerful method to resolve and quantify active sites in these materials. Phosphorus-31 is an ideal probe nucleus as it is 100% naturally abundant, has a nuclear spin number $I = 1/2$, and has a high gyromagnetic ratio. These nuclear properties make ^{31}P NMR spectroscopy a relatively sensitive technique despite the low concentrations of catalytic sites present in these zeolites, while the shortened acquisition times and high signal-to-noise (S/N) ratios compared to those for ^{119}Sn make this quantitative NMR technique more practical. A recent review by Zheng and co-workers provides an extensive summary of how trimethylphosphine (TMP) and various trialkylphosphine oxides have been used to study acid catalysts and highlights how NMR methods including $^{1}H-^{31}P$ heteronuclear correlation and $^{31}P-^{31}P$ double-quantum correlation spectroscopy have provided additional proximity information for these probe molecules adsorbed on Brønsted acid sites.[26] Trimethylphosphine oxide (TMPO) has been shown to effectively titrate and distinguish Brønsted acid sites with different acid strengths in aluminosilicates,[27−29] and theoretical studies have predicted the ability for TMP to characterize the strength of homogeneous Lewis acids.[30] Zhuang et al. used TMP to identify Brønsted and Lewis acidic sites in titanium-containing zeolite TS-1 and later used the conversion of adsorbed TMP to TMPO as a probe reaction for further characterization.[31,32] Here, we demonstrate that TMPO adsorption coupled with ^{31}P MAS NMR spectroscopy is a general method for distinguishing and quantitating the relative concentration of distinct active sites within Lewis acid zeolites, including Ti-, Hf-, and Zr-Beta, which have remained inaccessible to traditional MAS NMR analyses. The method allowed the elucidation of specific active sites in Sn-Beta for glucose isomerization and benzaldehyde-acetone aldol condensation reactions. Overall, this study demonstrates a robust method that allows for the identification of distinct sites in Lewis acid zeolites.

RESULTS AND DISCUSSION

Identification and Quantification of Tetrahedral Sn Sites in Sn-Beta. Phosphorus-31 MAS NMR spectra were acquired after dosing a representative Sn-Beta sample (Si/Sn molar ratio of 300, Sn-Beta-300a) with different loadings of TMPO using a dichloromethane (DCM) solvent-assisted technique (Figure 1). The TMPO occupancy at each site

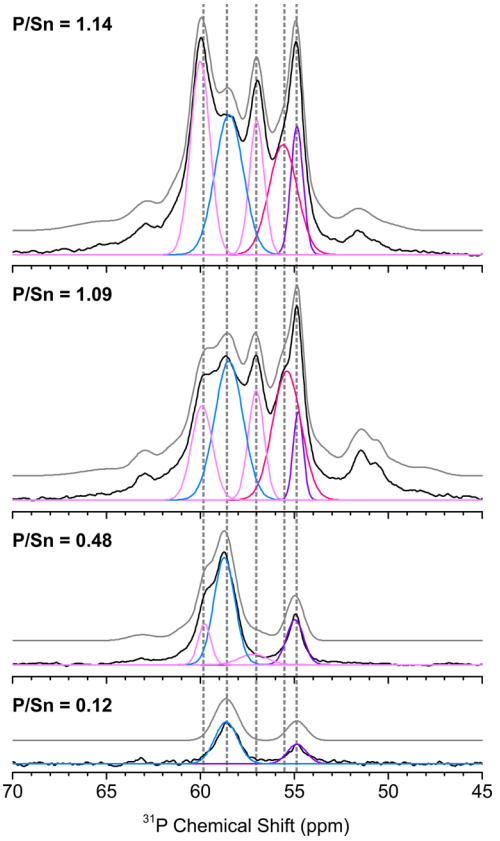

Figure 1. ^{31}P MAS NMR spectra ($\omega_0/2\pi(^{31}P)$ = 161.9 MHz (B_0 = 9.38 T), $\omega_r/2\pi$ = 10 kHz) of TMPO dosed on Sn-Beta-300a at different loading levels. Experimental NMR spectra are shown in black (lower traces), while the simulated spectra are shown in gray (upper traces). The gray dashed lines indicate the main resonance positions with corresponding Gaussian peak curves shown in light pink (δ_{iso} = 59.9 and 57.2 ppm), blue (δ_{iso} = 58.6 ppm), pink (δ_{iso} = 55.8 ppm), and violet (δ_{iso} = 54.9 ppm). Deconvolutions for minor peaks (≥61.3 ppm and ≤53.6 ppm) are not shown for clarity. Spinning sidebands appear outside the field of view.

(Table 1) was calculated from the relative peak area normalized by the total P and Sn contents measured by inductively coupled plasma mass spectrometry (ICP-MS). The narrow signals (<1.5 ppm, full width at half-maximum, fwhm) observed when TMPO is bound to Lewis acidic sites in Sn-Beta is a result of the low-defect zeolite pore structure that confines the TMPO molecules to specific geometries, providing a highly ordered chemical environment with a narrow range of chemical shifts associated with each type of Sn site. These confinement effects and the high sensitivity of ^{31}P NMR allow excellent distinction between TMPO molecules in different chemical environments.

DOI: 10.1021/acscatal.7b03533
ACS Catal. 2018, 8, 3076−3086

Table 1. TMPO Occupancy Normalized by Sn Content Determined from the Deconvolution of ^{31}P MAS NMR Spectra and Site Time Yields (STY) for Aqueous Glucose Isomerization and Aldol Condensation of Benzaldehyde and Acetone in Toluene for Sn-Beta Zeolites Prepared via Different Synthesis Conditions

		integrated ^{31}P NMR peak intensity (%) normalized by Sn content at each resonance (ppm)[c]											STY[d] (mol product)(mol Sn)$^{-1}$ h^{-1}	
catalyst[a]	TMPO/Sn ratio[b]	66.0	63.1	61.3	59.9	58.6	57.2	55.8	54.9	53.6	51.5	≤50.5	glucose isomerization	aldol condensation
Sn-Beta-300a	0.12					9			3				29.3	7.0
	0.48		2	5	6	24	3		8					
	1.09	3	3	5	13	26	12	25	6	5	7	5		
	1.14	3	5	5	24	25	13	20	10	4	4	1		
Sn-Beta-300b	0.97	2	3	4	17	21	16	7	16	5	4	1	22.0	7.1
Sn-Beta-200	0.96	3	3	5	7	20	14	10	23	3	7	2	25.4	5.8
Sn-Beta-100	0.83	3	7	3	10	17	11	10	13	4	4	1	11.3	5.1
Sn-Beta-300m	0.98	5	5	10	17	22	15	3	9	4	5	3	13.6	7.8
Sn-Beta-150m	1.07	3	4	6	14	23	20	5	13	5	11	2	9.5	7.8
^{119}Sn-Beta-300m	1.17	3	3	7	17	25	24	11	16	4	4	2	n.m.[e]	n.m.[e]

[a]Catalyst naming convention: Sn-Beta-X, where X is the Si/Sn molar ratio, a and b are duplicate syntheses, m stands for catalysts synthesized with Sn metal precursor. [b]From ICP-MS. [c]% ^{31}P integrated peak intensity at X ppm = (mol P/g-cat) (mol Sn/g-cat)$^{-1}$ (area % at δ = X ppm). Estimated error for these measurements is 10% of the reported area. [d]Site time yield (estimated error for these measurements is 10%). Reaction conditions and methods for calculating STY are given in the Experimental Procedures section of the Supporting Information. Product for glucose isomerization is fructose. Product for aldol condensation is benzalacetone. [e]Not measured.

The relative quantity of TMPO occupying different sites in the Sn-Beta zeolite is reflected by the integrated areas of the ^{31}P NMR peaks. At low TMPO loadings (e.g., TMPO/Sn molar ratio = 0.12), two resonances appear at δ_{iso} = 58.6 and 54.9 ppm at a ratio of ca. 3:1. When the TMPO dosing is increased to TMPO/Sn = 0.48, the areas of these two resonances increase while maintaining an approximately 3:1 ratio. New resonances with relatively low area (≤6%) are observed at δ_{iso} = 63.1, 61.3, 59.9, and 57.2 ppm. At TMPO loadings above unity (i.e., TMPO/Sn = 1.09 and 1.14), the ^{31}P NMR resonances at δ_{iso} = 59.9 and 57.2 ppm increase in intensity along with a new, relatively high intensity signal (20−25%) at δ_{iso} = 55.8 ppm. At these higher TMPO concentrations, additional low intensity signals (≤7%) appear at δ_{iso} = 66.0, 53.6, 51.5, and ≤50.5 ppm. Importantly, samples with TMPO/Sn > 1 contain an excess of TMPO relative to the quantity of Sn sites, so at least one of the observed signals in the ^{31}P NMR spectra must be generated by TMPO molecules that are not associated with Sn and/or by a second TMPO molecule bound to a Sn site that is already titrated.

The ^{31}P isotropic chemical shifts observed for TMPO adsorbed on Sn-Beta (δ_{iso} = 66.0 to 50.5 ppm) lie within the range expected for adducts formed between TMPO and either Brønsted or Lewis acids. TMPO adsorption studies on various amorphous and microporous crystalline aluminosilicates with Brønsted acidity featured ^{31}P NMR signals in the range from δ_{iso} = 75 to 50 ppm,[28,29] and TMPO bound to Lewis acid sites in TS-1 have been assigned a chemical shift of 53.7 ppm.[32] Density functional theory (DFT) calculations predicted that resonance frequencies of ^{31}P nuclei in Lewis acid-TMPO adducts of B, Al, and Ti chloro and fluoro compounds lie between δ_{iso} = 55 and 38 ppm.[28] The ^{31}P magnetic shielding for TMPO adsorbed in a zeolite is sensitive to its local chemical environment as dictated by the nature of the active site and the topology of the pore. In the context of molecular orbital theory, a stronger binding Lewis acid will pull more electron density from the highest occupied molecular orbital (HOMO) of the TMPO oxygen molecule to the lowest unoccupied molecular orbital (LUMO) of the Lewis acid, affecting the magnetic field experienced at the phosphorus nucleus.[33] However, the interaction of the TMPO with different Sn environments such as T-site locations, coordination number, and orientation within unique pore geometries can influence the ^{31}P chemical shift when the TMPO is bound to a Lewis acid, making it difficult to make definitive assignments of acid strength exclusively from changes in chemical shift.

A series of control samples (Figure S1) was used to assist in the assignment of ^{31}P MAS NMR resonances. In agreement with previous studies of TMPO adsorbed on HZSM-5 and MCM-41,[34] the ^{31}P MAS NMR spectrum of TMPO dosed on Si-Beta consisted of a single resonance at δ_{iso} = 41 ppm corresponding to physisorbed TMPO. The broad signal observed for this species, with a fwhm of 9 ppm, reveals that physisorbed TMPO is more disordered within the zeolite pore structure than TMPO coordinated to Lewis acid sites. No additional resonances appear for Si-Beta containing extra-framework SnO_2 clusters, indicating that these species do not bind TMPO to a significant degree. The ^{31}P MAS NMR spectrum of TMPO dosed on a highly defective Si-Beta obtained by dealumination of Al-Beta (Si/Al molar ratio of 12.5) consisted of a broad resonance (fwhm = 11.3 ppm) at δ_{iso} = 43.5 ppm. Importantly, NMR spectra of these controls do not show resonances centered at frequencies higher than δ_{iso} = 50 ppm, such as those present in the NMR spectra of Sn-Beta samples, which we have assigned to TMPO interacting with Sn sites in framework positions.

The interaction of water molecules with TMPO and/or the Sn site(s) was ruled out using ^{1}H MAS NMR spectroscopy. Clean dosed samples showed a single resonance at δ_{iso} = 1.5 ppm corresponding to the methyl protons in TMPO (Figure S2a). Remnant fluoride ions from synthesis that may remain within the zeolite even after washing and calcination could also affect TMPO/Sn interactions.[35] Fluorine-19 MAS NMR spectra (Figure S2b) showed only a minute quantity of SiF_6 species present in the zeolite. As such, we concluded that TMPO/F^- or TMPO/Sn/F^- complexes are not associated with the major resonances observed by ^{31}P MAS NMR spectroscopy. It cannot be excluded, however, that these species correspond to the resonances featuring low TMPO occupancy, such as at δ_{iso} = 66.0, 63.1, or ≤50.5 ppm.

DOI: 10.1021/acscatal.7b03533
ACS Catal. 2018, 8, 3076−3086

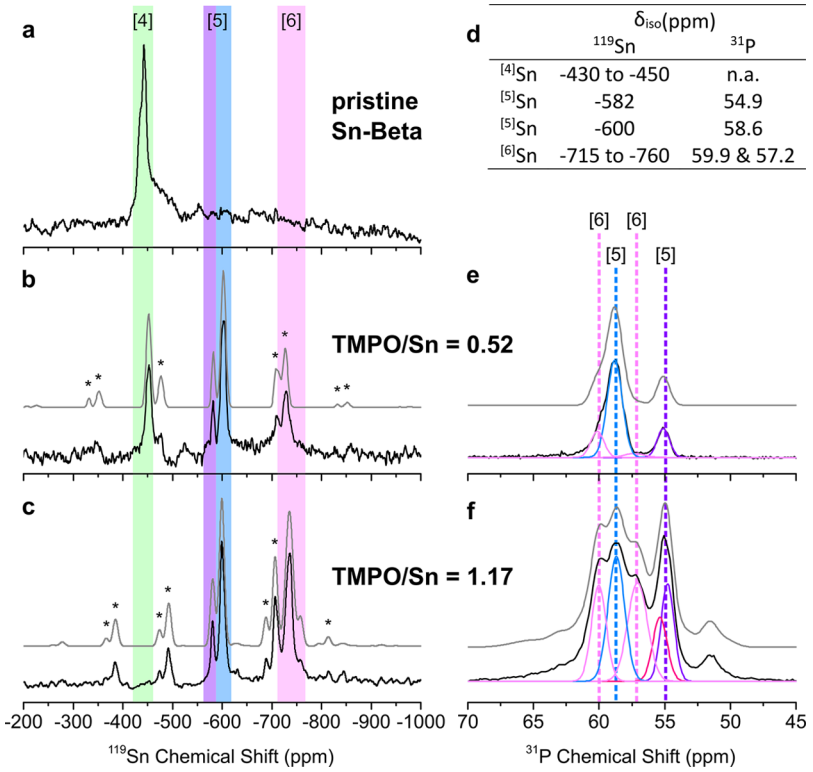

Figure 2. ^{119}Sn ($\omega_0/2\pi(^{119}\text{Sn})$ = 111.9 MHz (B_0 = 7.05 T), $\omega_r/2\pi$ = 12 kHz) (a–c) and ^{31}P ($\omega_0/2\pi(^{31}\text{P})$ = 161.9 MHz (B_0 = 9.38 T), $\omega_r/2\pi$ = 10 kHz) (e,f) MAS NMR spectra of ^{119}Sn-Beta-300m: (a) pristine sample. (b and e) Dosed with TMPO/Sn = 0.52. (c and f) Dosed with TMPO/Sn = 1.17. Spinning sidebands in the ^{119}Sn spectra are marked with asterisks. Experimental NMR spectra are shown in black (lower traces), while the simulated spectra are shown in gray (upper traces). Peak fitting results are given in Table S1. Gaussian peak curves for the ^{31}P NMR spectra are shown in color according to their assignment (Figure 1). Shaded regions in the ^{119}Sn spectra correspond to regions of $^{[4]}$Sn (green), $^{[5]}$Sn (violet/blue), and $^{[6]}$Sn (pink). (d) Peak assignments. ^{119}Sn MAS NMR spectrum shown in b was acquired using a MAS frequency of 14 kHz.

The combined results from the incremental dosing of Sn-Beta and control experiments, along with reported assignments from the literature, were used to make preliminary assignments for the ^{31}P MAS NMR resonances. Given that the resonances at δ_{iso} = 58.6 and 54.9 ppm appear at low TMPO loadings and are selectively titrated with increased dosing, we believe that they correspond to adducts composed of one TMPO molecule bound to one framework Sn site. Based on assignments reported in the literature, ^{31}P NMR peaks between δ_{iso} = 66.0 and 61.3 ppm most likely correspond to TMPO interacting with Brønsted acidic sites.[26] These assignments are in agreement with our results showing low occupancy for these sites, which could arise from a small number of silanol groups or other defect sites that possess weak Brønsted acidity.[22,36,37] The ^{31}P resonances at δ_{iso} = 53.6, 51.5, and ≤50.5 ppm account for a relatively small portion of TMPO molecules and appear only at higher concentrations, which could be due to either TMPO interacting with a weaker or minor site in the zeolite or TMPO binding at an existing Sn-TMPO adduct. The resonances at δ_{iso} = 59.9, 57.2, and 55.8 ppm accounted for a significant fraction of TMPO; however, definitive assignment could not be made from the incremental dosing experiments alone and required correlations with other NMR measurements (vide infra).

Peak assignments were further refined by using data from ^{119}Sn MAS NMR spectra of ^{119}Sn-enriched Sn-Beta samples with a Si/Sn ratio of ∼300 (^{119}Sn-Beta-300m, synthesized with ^{119}Sn-enhanced metal precursor) dosed with TMPO (Figure 2, Table S1). As expected, pristine, dehydrated ^{119}Sn-Beta-300m exhibits sharp ^{119}Sn resonances at δ_{iso} = −434 and −443 ppm corresponding to two different four-coordinate, pseudotetrahedral Sn ($^{[4]}$Sn) environments in the zeolite framework with approximately a 30:70 ratio (Figure 2a). In addition to these two sharp resonances, a broad component spanning the $^{[4]}$Sn region was observed, which could be potentially attributed to disordered Sn distributed randomly throughout the framework. When TMPO was adsorbed onto ^{119}Sn-Beta-300m at a ratio of TMPO/Sn = 0.52 (Figure 2b), the ^{119}Sn MAS NMR spectrum showed a single peak at δ_{iso} = −450 ppm corresponding to pseudotetrahedral Sn and two new signals at δ_{iso} = −600 and −582 ppm assigned to penta-coordinated Sn ($^{[5]}$Sn).[38,39] Importantly, the resonances at δ_{iso} = −600 and −582 ppm appeared at a 3:1 ratio and could be clearly assigned to the two sites with ^{31}P MAS NMR resonances at δ_{iso} = 58.6 and 54.9 ppm, respectively, which appeared in approximately the same ratio (4:1, Figure 2e). The spinning sideband manifolds were accounted for in these area ratios due to a considerable chemical shift anisotropy (CSA) contribution observed experimentally and our inability to attenuate the spinning sidebands at moderate spinning frequencies. A minor contribution of six-coordinate Sn ($^{[6]}$Sn, ∼5%, estimated from experiments acquired using multiple spinning frequencies at both 7.1 and 11.7 T) was observed for this sample. Unfortunately, the low S/N and appreciable spinning side bands from the $^{[5]}$Sn signals did not allow us to determine the exact chemical shift or concentration of this $^{[6]}$Sn site.

Phosphine oxides are known to form 2:1 Sn-TMPO adducts with organotin chlorides in the presence of excess phosphine

DOI: 10.1021/acscatal.7b03533
ACS Catal. 2018, 8, 3076−3086

oxide.[38] At higher TMPO loadings, it is likely that two TMPO molecules will coordinate to a single Sn center, resulting in $^{[6]}$Sn that will appear at low frequency in the ^{119}Sn NMR spectrum. Accordingly, increasing the TMPO loading to TMPO/Sn = 1.17 resulted in the appearance of a high intensity resonance at δ_{iso} (^{119}Sn) = −735 ppm corresponding to hexa-coordinated, pseudo-octahedral Sn (Figure 2c). The ^{31}P (Figure 2f) and ^{119}Sn MAS NMR spectra provide TMPO occupancies and relative $^{[5]}$Sn speciation that are consistent with our preliminary peak assignments: the ratio of peak areas at δ_{iso} (^{119}Sn) = −600/−582 ppm and δ_{iso} (^{31}P) = 58.6/54.9 ppm are generally consistent at ca. 3:1 to 2:1. As expected, no four-coordinate Sn remains at this excess titration level.

Introduction of a second TMPO molecule to an existing Sn-TMPO adduct (corresponding to either δ_{iso} (^{31}P) = 58.6 or 54.9 ppm) should theoretically result in two new ^{31}P signals: the first signal being the new δ_{iso} (^{31}P) of the original TMPO molecule now featuring a new chemical environment arising from the presence of a second TMPO molecule in close proximity and the second signal being for the second TMPO molecule. It is important to note that it is impossible to know directly from our NMR results whether TMPO at the $^{[5]}$Sn site that becomes doubly titrated originally had a chemical shift at δ_{iso} (^{31}P) = 58.6 or at 54.9 ppm. To further probe which ^{31}P resonances correspond to the TMPO molecules contributing to the $^{[6]}$Sn signal, we conducted a ^{31}P double quantum-single quantum (DQ-SQ) NMR experiment on the TMPO/Sn = 1.17 sample (Figure S3). Despite the low S/N observed even after 670 h of continuous acquisition, the ^{31}P DQ-SQ NMR spectrum clearly shows that the ^{31}P chemical shifts at δ_{iso} = 59.9 and 57.2 ppm are correlated and confirms that these two species are bound to the same $^{[6]}$Sn Lewis acid site. These signals are present approximately in a 1:1 ratio in the ^{31}P NMR spectra of the TMPO/Sn = 1.17 sample, as well as in the ^{31}P NMR spectra of other samples dosed with TMPO/Sn ratios of ∼1 (vide infra). With this information in hand, we note that the ^{31}P NMR spectrum of the TMPO/Sn = 0.52 sample also featured these two signals (albeit with low intensities), which is consistent with the small amount of $^{[6]}$Sn present in the corresponding ^{119}Sn MAS NMR spectrum. The ^{31}P DQ-SQ NMR spectrum also confirmed our assignments of δ_{iso} (^{31}P) = 58.6 and 54.9 ppm to $^{[5]}$Sn environments, as these chemical shifts were only observed in low intensity along the DQ-SQ diagonal (i.e., they are not correlated to one another or to other ^{31}P resonances). Unfortunately, the ^{31}P DQ-SQ NMR results could not discriminate between single or double TMPO binding environments for the remaining ^{31}P signals, including the relatively intense signal at δ_{iso} (^{31}P) = 55.8 ppm, due to the low sensitivity for this experiment.

In theory, the total amount of TMPO obtained from adding the ^{31}P MAS NMR peak areas from the assigned $^{[5]}$Sn and $^{[6]}$Sn sites (i.e., δ_{iso} = 58.6, 54.9, 57.2 (or 59.9), and 55.8 ppm) for a fully titrated Sn-Beta sample should equal the total amount of framework Sn sites present in the sample. When this calculation was performed using the TMPO/Sn = 1.17 sample, the sum accounted only for 69−76% of the total Sn content as compared to the value obtained with elemental analysis. We also found that the fraction of $^{[4]}$Sn in the TMPO/Sn = 0.52 sample (Figure 2b) calculated from the ^{119}Sn MAS NMR spectrum was less than the expected value. This disparity indicated that the ^{119}Sn-Beta-300m sample had at least 20% of disordered $^{[4]}$Sn (possibly appearing as a broad resonance between δ_{iso} (^{119}Sn) = −450 and −500 ppm, Figure 2a) or that the sample contained extra-framework SnO_2 (δ_{iso} = −603.4 ppm, Ω = 125 ppm and κ = −1).[40] However, no evidence of resonances associated with $^{[6]}$Sn were observed in the ^{119}Sn MAS NMR spectrum of the pristine sample. These discrepancies could be due to the low loading (∼1 wt % ^{119}Sn) of Sn within the zeolite, whereby significant continuous averaging of the ^{119}Sn NMR spectra (100 to 200 h) is required to reveal the dominant Sn coordination environments within Sn-Beta. The three main species found here depending on TMPO loading exhibited small to moderate chemical shift anisotropies (i.e., $^{[4]}$Sn/$^{[5]}$Sn/$^{[6]}$Sn exhibited spans of ∼150−200 ppm/∼ 400 ppm/ ∼ 200−300 ppm, respectively). As a result of the complex ^{119}Sn NMR results, measurements at multiple spinning frequencies (8 to 14 kHz) and multiple magnetic field strengths (B_0 = 7.05 to 21.1 T) were used to interpret these data. These challenges emphasize the risks associated with using ^{119}Sn MAS NMR spectroscopy alone to characterize Sn-Beta materials and underscore the need to develop complementary characterization techniques.

Comparison of Site Speciation in Sn-Beta Samples Synthesized under Different Conditions. A series of Sn-Beta zeolites with varying Si/Sn ratios and metal precursors was synthesized in fluoride media to generate materials with different Sn speciation and catalytic activity.[41,42] These materials exhibited the physical properties characteristic of Sn-Beta crystals, including nearly identical powder X-ray diffraction (PXRD) patterns (Figure S4), crystal morphologies (Figure S5), nitrogen adsorption and desorption isotherms (Figure S6), micropore volumes and BET surface areas (Table S2). Diffuse-reflectance ultraviolet/visible (DRUV) spectroscopy of these materials showed bands at approximately 200 nm, indicative of tetrahedrally incorporated Sn species (Figure S7). Of all DRUV spectra, that of Sn-Beta-100 with Si/Sn = 100 exhibited the clearest sign that extra-framework species were present, as signified by a low intensity band around 270 nm.[43] As expected for materials with different site speciation, the ^{31}P NMR spectra (Figure S8) of the various TMPO-dosed Sn-Beta samples (TMPO/Sn molar ratio ∼1) show different proportions of the integrated peak areas (Table 1).

According to our assignments, the total amount of framework Sn sites should be represented by the sum of the peak areas for resonances at δ_{iso} = 58.6, 57.2 (or 59.9), 54.9, and possibly 55.8 ppm. For the samples tested, this value amounted to 50 to 76% (±5%) of the total Sn in the sample (including the area at δ_{iso} = 55.8 ppm). This result implied that there is a non-negligible amount of extra-framework oxide species, which typically cannot be detected by DRUV (Figure S7) but can be observed as small tin oxide nanoparticles using a backscatter detector in scanning electron microscopy (SEM).[42] Importantly, our framework content agrees with a study by Harris and co-workers using similar Sn-Beta materials that showed metal framework incorporation of up to 88% as determined by pyridine and acetonitrile titrations.[20]

Relating Catalytic Activity to Site Distributions. Unlike prior characterization techniques, our TMPO dosing method allows correlating catalytic activity with distinct sites in the zeolite framework. We compared the catalytic activity of Sn-Beta samples using two different reactions, namely glucose isomerization to fructose in water and aldol condensation of benzaldehyde with acetone in toluene. These reactions have been shown to turnover at framework Sn sites; however, the exact configuration of the active site has remained unclear.

DOI: 10.1021/acscatal.7b03533
ACS Catal. 2018, 8, 3076−3086

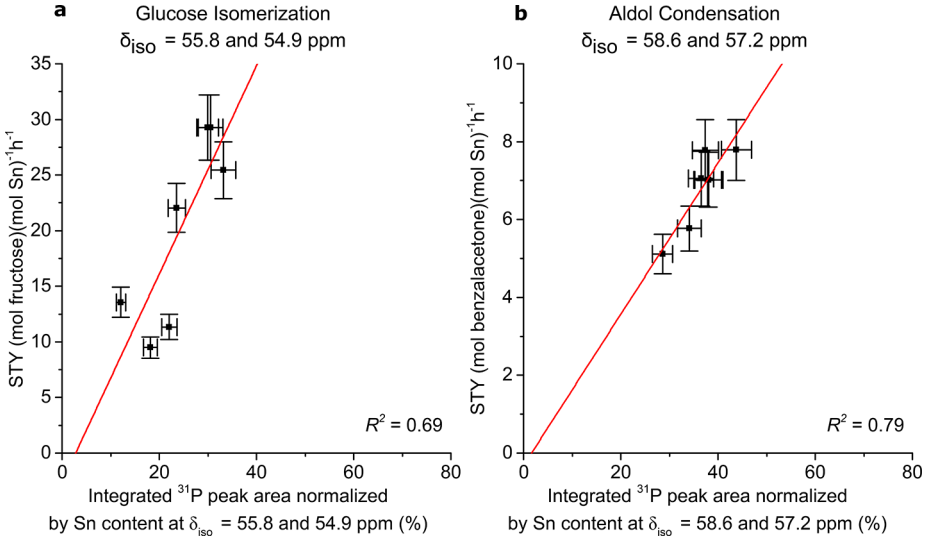

Figure 3. Site time yield (STY) for (a) glucose isomerization in water and (b) aldol condensation of benzaldehyde and acetone in toluene catalyzed by different Sn-Beta catalysts plotted against the percent integrated ^{31}P peak area normalized by P and Sn content at (a) δ_{iso} = 55.8 and 54.9 ppm and (b) δ_{iso} = 58.6 and 57.2 ppm. The integrated ^{31}P peak area is related to the concentration of TMPO bound to Sn sites with a particular geometry: % Integrated ^{31}P peak area at X ppm = (mol TMPO/g-cat) (mol Sn/g-cat)$^{-1}$ (area % at δ_{iso} = X ppm). The red lines are linear fits of the data.

Catalytic activity was tested using a packed bed liquid flow reactor as described in the Experimental Procedures section of the Supporting Information, and site-time-yields (STY) for each reaction were normalized by the total Sn content measured by elemental analysis (Table 1 and Figure S9).

Glucose Isomerization. The rate of glucose isomerization for Sn-Beta ranged from 9.5 to 29.3 (mol fructose) (mol total Sn)$^{-1}$h^{-1}, with catalysts synthesized using $SnCl_2{\cdot}2H_2O$ as the Sn precursor typically showing higher activity than those synthesized using Sn metal dissolved in HCl. Additionally, catalysts with higher Sn loadings (Sn-Beta-100 and Sn-Beta-150m) appeared to be less active when normalized by total Sn content, suggesting that less of the metal was incorporated into the zeolite in configurations active for glucose isomerization. This effect is not surprising considering the thermodynamic limitations of incorporating a high Sn content (100:1 Si/Sn molar ratio) via hydrothermal synthesis.[42] Indeed, the crystallization time required for Sn-Beta-100 was 32 days compared to 7 days for Sn-Beta-300b.

To establish a relationship between Sn speciation in Sn-Beta and the glucose isomerization activity, STYs were plotted against the % integrated peak area normalized by total Sn content (Figure S10). Resonances used for these comparisons were chosen according to our assignments for $^{[5]}$Sn and $^{[6]}$Sn (*vide supra*). Note that if a particular Sn configuration is responsible for catalytic turnover, then the addition of the integrated peak areas from the ^{31}P spectra corresponding to 100% of the $^{[5]}$Sn area and 50% of the $^{[6]}$Sn area (i.e., the area of only one of the two TMPO resonances from the pair) should correlate with the reaction rate. Since the NMR analysis alone could not conclusively inform which $^{[5]}$Sn site gained a second TMPO molecule to produce the δ_{iso} (^{31}P) = 59.9/57.2 ppm pair, we considered both options: (a) δ_{iso} (^{31}P) = 54.9 + 59.9/57.2 ppm and (b) δ_{iso} (^{31}P) = 58.6 + 59.9/57.2 ppm. The resonance at 55.8 ppm was included in the analysis for other combinations because it contributed a significant fraction of the ^{31}P peak area for several samples. Other resonances with relatively low occupancy were not considered in site combinations due to their small contribution to the total area relative to the increase in error from adding more sites. Nonetheless, all the trends from individual resonances are plotted for completeness in the Supporting Information (Figures S11 and S12). One would expect that if a unique site titrated by TMPO were responsible for catalytic activity, then a plot of the STY versus the ^{31}P peak areas associated with that site would exhibit a positive linear trend that intersects the origin. Such a trend was only observed for glucose isomerization when combining the contributions from the ^{31}P NMR resonances at δ_{iso} = 55.8 and 54.9 ppm (Figure 3a). This combination yielded a relatively good linear fit with an R^2 value of 0.69 and intersected the origin within error. Including either doubly titrated site, δ_{iso} = 59.9 or 57.2 ppm (Figure S10e and h), with this set also resulted in linear fits, but the *x*-intercepts were significantly offset, suggesting these combinations over counted sites (i.e., it included sites that were not active). Similar trends were obtained when combining all possible sites (both $^{[5]}$Sn sites and one $^{[6]}$Sn, Figure S10b and c). The analysis for a single $^{[5]}$Sn site at δ_{iso} = 54.9 ppm (not including 55.8 ppm), a single $^{[5]}$Sn site at δ_{iso} = 58.6 ppm, or the combination of the $^{[5]}$Sn site at δ_{iso} = 58.6 ppm plus either of the $^{[6]}$Sn sites at δ_{iso} = 59.9 or 57.2 ppm did not produce linear fits.

From these data, we concluded that the active site for glucose isomerization corresponds to the site(s) titrated by TMPO having a ^{31}P resonance located at δ_{iso} (^{31}P) = 55.8 and 54.9 ppm. The concentration of this active site ranged from 12 to 33% of the total Sn content for our samples, which is in remarkable agreement with the concentrations of glucose isomerization active sites (13−33%) calculated by Harris et al. using acetonitrile adsorption and FTIR spectroscopy for a variety of fluoride-synthesized Sn-Beta samples.[20] These data also suggest that the $^{[6]}$Sn with δ_{iso} (^{31}P) = 59.9/57.2 ppm are not associated with the $^{[5]}$Sn peak at δ_{iso} (^{31}P) = 54.9 ppm. While it is clear that the TMPO resonance that appears at δ_{iso} (^{31}P) = 55.8 ppm is important for reactivity, we cannot conclusively assign its identity due to the low S/N and high error in our ^{119}Sn NMR measurements. However, we hypothesize that it likely arises either from a $^{[6]}$Sn environment resulting from the double titration of the site with δ_{iso} (^{31}P) =

DOI: 10.1021/acscatal.7b03533
ACS Catal. 2018, 8, 3076−3086

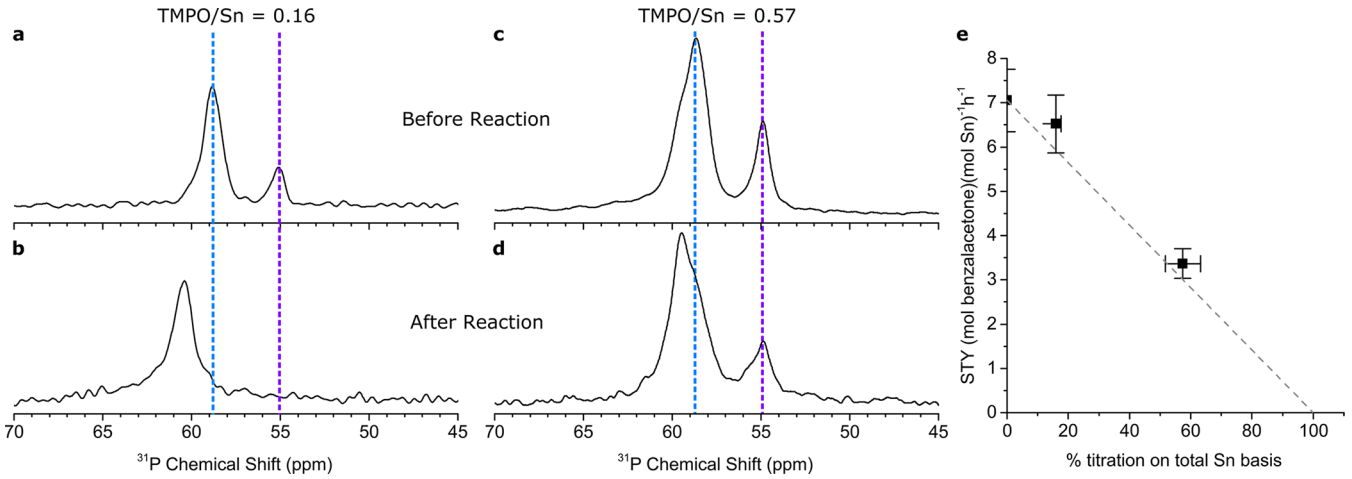

Figure 4. (a–d) ^{31}P MAS NMR spectra ($\omega_0/2\pi(^{31}P)$ = 161.9 MHz (B_0 = 9.38 T), $\omega_r/2\pi$ = 10 kHz) of TMPO dosed on Sn-Beta-300b before (a and c) and after (b and d) it was used as the catalyst for aldol condensation of benzaldehyde and acetone in a packed bed reactor, as shown in Figure S17. TMPO/Sn = 0.16 for a and b and TMPO/Sn = 0.57 for c and d. Spinning sidebands appear outside the field of view. Dashed lines at δ_{iso} = 58.6 ppm (blue) and δ_{iso} = 54.9 ppm (violet) are used as a guide to show shifts after reaction. (e) STY for aldol condensation of benzaldehyde and acetone plotted against the % titration on a total Sn basis. The dashed gray line in d is the theoretical linear titration curve where 0% titration results in full activity and 100% titration results in no activity.

54.9 ppm or from a separate $^{[5]}$Sn site that has similar reactivity to the site at δ_{iso} (^{31}P) = 54.9 ppm. Importantly, these assignments are consistent with the ratio of the two $^{[4]}$Sn sites (δ_{iso} = −443 and −434 ppm, 70:30) seen in the ^{119}Sn MAS NMR spectra of pristine ^{119}Sn-Beta-300m. For the TMPO analysis of this sample, the ratio of integrated peak area for sites associated with δ_{iso} (^{31}P) = 58.6 and 59.9/57.2 ppm versus sites associated with δ_{iso} (^{31}P) = 55.8 and 54.9 ppm is ca. 2:1. Taken together, these data suggest that the ^{31}P resonances at δ_{iso} (^{31}P) = 58.6 and 59.9/57.2 ppm, which are assigned to $^{[5]}$Sn and $^{[6]}$Sn, respectively, originate from the $^{[4]}$Sn site at δ_{iso} (^{119}Sn) = −443 ppm. Analogously, the ^{31}P resonances at δ_{iso} (^{31}P) = 55.8 and 54.9 ppm can be attributed to TMPO binding the $^{[4]}$Sn site at δ_{iso} (^{119}Sn) = −433 ppm.

Aldol Condensation. TMPO analysis was also conducted to determine the active site speciation for aldol condensation of benzaldehyde (BA) and acetone in toluene. The STYs for this reaction ranged from 5.1 to 7.8 (mol BA) (mol Sn)$^{-1}$h^{-1}, with catalysts synthesized with a Sn metal precursor featuring the highest activity normalized by total Sn content. We suspected that the active site for aldol condensation could differ from that for glucose isomerization due to the different reactivity trends exhibited by Sn-Beta samples for the two reactions (Figure S9). For example, while Sn-Beta-150m featured the lowest activity for glucose isomerization, it showed the highest activity for aldol condensation. Glucose isomerization and aldol condensation proceed via different mechanisms: the former involves a ring-opening step followed by intramolecular hydride transfer,[44] while the latter requires enolate formation at the metal site.[45] Thus, it is entirely possible that different tetrahedral-Sn site geometries are responsible for catalytic activity for each reaction. Dijkmans et al. reported similar findings where the relative activity of Sn-Beta samples synthesized by different postsynthetic techniques varied depending on the test reaction used.[46]

Plots of the STY for aldol condensation versus the peak areas of different ^{31}P MAS NMR resonances showed drastically different trends compared to those found for glucose isomerization (Figures S13–S15). Specifically, linear correlations were only found for the combination of the $^{[5]}$Sn site at δ_{iso} = 58.6 ppm and either δ_{iso} = 59.9 or 57.2 ppm of the $^{[6]}$Sn site pair. As shown in Figure 3b, the trend for combining δ_{iso} = 58.6 and 57.2 ppm fits especially well with an R^2 value of 0.79 and a *y*-intercept at the origin. Importantly, these results support our hypothesis that $^{[6]}$Sn TMPO sites at δ_{iso} (^{31}P) = 59.9 and 57.2 ppm correspond to the double titration of the δ_{iso} (^{31}P) = 58.6 ppm site. The goodness of fit worsens (R^2 = 0.49) and the *y*-intercept increases when using the peak area for δ_{iso} = 59.9 ppm instead of 57.2 ppm for the $^{[6]}$Sn position in combination with the $^{[5]}$Sn at δ_{iso} = 58.6 ppm, likely because of the poor fitting of the peak at 59.9 ppm for one of the samples (Sn-Beta-300a, TMPO/Sn = 1.14). This sample had a much higher value (24%) for the δ_{iso} = 59.9 ppm peak area than that for the slightly lower loading on the same zeolite (Sn-Beta-300a, TMPO/Sn = 1.09, 13%). When this potential outlier was removed, the fit improved to R^2 = 0.81, and the slope and *y*-intercept more closely matched those seen for the fit using the δ_{iso} = 57.2 ppm values. Indeed, a careful balance of TMPO loading must be kept in order to fully titrate the tetrahedral sites without introducing new environments that convolute the spectra and prevent proper analysis.

We reasoned that if the $^{[5]}$Sn site at δ_{iso} (^{31}P) = 58.6 ppm is active for the aldol condensation, then direct titration of these sites with TMPO should result in a proportional decrease in catalytic activity. Titration experiments were conducted by dosing Sn-Beta-300b at two TMPO loadings, 16 and 57%, before testing the catalytic activity for aldol condensation in a packed bed reactor. ICP-MS experiments performed post-reaction showed that over 97% of the dosed TMPO molecules remained bound to the catalyst after reaction. However, ^{31}P MAS NMR spectra of the samples acquired after reaction (Figures 4b and d) showed changes in the environment of the bound TMPO compared to the prereaction spectra (Figures 4a and c), with a large fraction of the total integrated signals appearing at frequencies greater than 59 ppm. These changes can be attributed to deviations from the ideal geometry for TMPO-Sn complexes that could be caused either by alterations to the zeolite structure during reaction or by the presence of adsorbed compounds that remained in the pores after reaction.

DOI: 10.1021/acscatal.7b03533
ACS Catal. 2018, 8, 3076–3086

Thermogravimetric analysis (TGA) of the 16% TMPO titration catalyst postreaction showed a 2.3 wt % loss between 423 and 913 K (Figure S16), confirming that organic deposits remained occluded in the pores after drying. Additionally, we were unable to rule out the possibility that a TMPO molecule originally adsorbed at a specific site (e.g., the δ_{iso} = 54.9 ppm site in the 16% titration sample) could desorb and then readsorb at a different location in the material during reaction, since the experiments were conducted at elevated temperatures (383 K) in organic solvent (toluene). The steady state STYs for Sn-Beta samples titrated with TMPO at 16 and 57% decreased by 7.5 and 52%, respectively, compared to the nontitrated control sample (Figures 4e and S17). This decrease in activity can be attributed to TMPO molecules binding to active sites and preventing their participation in catalysis. Since the post-reaction characterization showed that TMPO remained in the zeolite throughout the reaction but could not corroborate which sites remained titrated (and we do not know if a site can remain active while singly titrated as opposed to doubly titrated), we could not explicitly correlate the drop in activity to the titration of a specific site. However, these results confirm that TMPO must bind to active sites, thus validating our TMPO-based method to investigate active site speciation.

Discussion of Active Site Assignments for Sn-Beta. The difference in Sn-Beta active site assignment for glucose isomerization and aldol condensation is striking and significant. The current results are especially illuminating, as many theoretical and experimental researchers have previously proposed that the same site, a hydrolyzed "open" site, is the catalytic site for both of these reactions. This hypothesis cannot account for the activity for both types of reactions discussed in this research, as Sn sites corresponding to δ_{iso} (^{31}P) = 58.6 and 59.9/57.2 ppm, i.e., δ_{iso} (^{119}Sn) = −600 ppm, in our Sn-Beta zeolites are shown to catalyze aldol condensation while sites corresponding to δ_{iso} (^{31}P) = 55.8 and 54.9 ppm, i.e., δ_{iso} (^{119}Sn) = −582 ppm, are active for glucose isomerization. The molecular connectivity of tetrahedral Sn centers is important and a widely debated topic in the field of Lewis acid zeolites. The question of whether a fully connected distorted tetrahedron (closed site) or a singly hydrolyzed Si−O−M (open site) is the more active site for various reactions has been addressed several times in the open literature.[19,23,47−50] Most studies have indicated that open sites are the active sites for glucose isomerization, as these configurations possess greater flexibility that reduces geometric distortion energy penalties for transition state formation and have added functionality due to the formation of metal hydroxy and silanol groups.[51] However, a recent study by Ivanova and co-workers[14] indicated that the experimental evidence for assigning a ^{119}Sn MAS NMR resonance at δ_{iso} = −423 ppm to an "open" configuration may be due to incomplete drying of the samples before analysis. Our TMPO dosing method is conducted under anhydrous conditions to prevent the interference of water on TMPO-Sn interactions, and the pretreatment conditions (573 K, 50 mTorr, > 12 h) would likely condense any open sites that would have formed in the materials after calcination. Therefore, we hypothesize that the ^{31}P MAS NMR resonances at δ_{iso} = 58.6 ppm and δ_{iso} = 54.9 ppm correspond to TMPO bound to Sn atoms present in different crystallographic positions, or T-sites, in the framework. First-principle calculations on cluster models of Sn-Beta with dehydrated closed sites performed by Wolf and co-workers[50] show that T-site dependence alone can explain experimentally observed ^{119}Sn MAS NMR chemical shifts. Additionally, several studies focused on DFT calculations have shown that local geometry influences the substitution of Lewis acidic heteroatoms into siliceous zeolite frameworks[52−54] and that the acidity of the site as measured by probe molecule binding will depend on the T-site location.[55] Although we expect our materials to contain only closed sites before analysis via the TMPO method, it is entirely possible for water to hydrolyze Si−O−Sn bonds during reaction to form open sites *in situ*. This is especially relevant for glucose isomerization where the solvent is water but might not be a major factor for the aldol condensation reaction carried out in toluene. DFT calculations of Sn-Beta zeolites have shown that the thermodynamic favorability of forming an open site depends on the T-site position.[55] Thus, the ^{31}P MAS NMR resonances appearing at δ_{iso} = 55.8 and 54.9 ppm, which were the only signals correlated with glucose isomerization activity, likely represent a TMPO molecule titrating a Sn site located at a T-site that is more prone to form an open site. This hypothesis resolves the contradictions on this topic found in the literature and is consistent with a recent study by Gounder and co-workers showing via coupled ^{119}Sn DNP NMR measurements and DFT calculations that tetrahedral Sn sites in Sn-CHA are closed when dehydrated and hydrolyze upon hydration.[25]

Probing the Acid Sites of Lewis Acid Zeolites with Other Heteroatoms. We demonstrate the general applicability of our method to probe a wide range of Lewis acid heteroatoms by analyzing Ti-, Zr-, and Hf-Beta samples. The ^{31}P MAS NMR spectra shown in Figure 5 demonstrate that

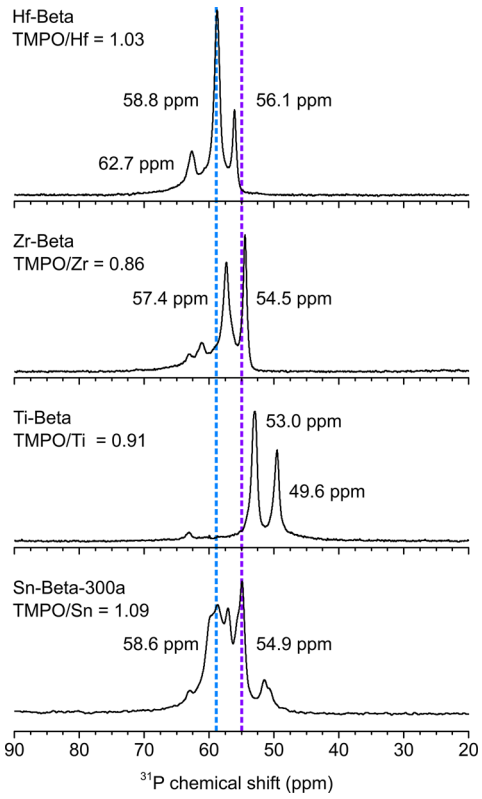

Figure 5. ^{31}P MAS NMR spectra ($\omega_0/2\pi$(^{31}P) = 202.4 MHz (B_0 = 11.75 T), $\omega_r/2\pi$ = 10 kHz) of TMPO dosed on Lewis acid zeolites with different heteroatoms at a TMPO/M ratio of approximately 1.0. The dashed lines mark the resonance positions in Sn-Beta at δ_{iso} = 58.6 ppm (blue) and 54.9 ppm (violet). Chemical shifts for all materials are written next to their respective resonances.

DOI: 10.1021/acscatal.7b03533
ACS Catal. 2018, 8, 3076−3086

TMPO adsorption can resolve at least two distinct metal sites in the range of δ_{iso} ~60 to 50 ppm for all three framework heteroatoms. Additional resonances at frequencies higher than δ_{iso} = 60 ppm appear with relatively small integrated peak areas that, similar to the Sn-Beta samples, could be due to Brønsted acidity in these Lewis acid zeolites. The variability of the resulting ^{31}P MAS NMR chemical shifts (up to 5.6 ppm difference between materials) suggests unique interactions between TMPO and the Lewis acid sites in these materials, which is expected since the electronic structures of the framework metal centers will vary depending on heteroatom identity.[56] This effect is also consistent with reactivity studies showing a different order of catalytic activity for Sn, Ti, Zr, and Hf sites depending on the reaction used. For example, for the isomerization of lactose, the initial turnover rates for Sn-Beta are 60 times higher than those for Ti-Beta.[57] In addition, the activation energy of Ti-Beta for the Meerwein–Ponndorf–Verley (MPV) reduction of methyl levulinate was 69 kJ/mol compared to 52 kJ/mol for the other M-Betas.[58] In the case of olefin epoxidation catalyzed by M-Beta zeolites, Bregante and Flaherty[59] demonstrated that activation enthalpies are correlated with two experimental descriptors of Lewis acid strength: heat of adsorption for acetonitrile and the ligand to metal charge transfer energy between the dioxygen reactive intermediates and the metal center. The periodic trends observed for these descriptors in the group IV M-Betas share similarities with the ^{31}P NMR chemical shift of adsorbed TMPO: the value of the descriptors increases going down the group in the periodic table, with those for Ti-Beta differing significantly from the relatively similar values determined for Hf- and Zr-Beta.

While further studies are needed to corroborate if ^{31}P chemical shifts of adsorbed TMPO can serve as a robust descriptor for Lewis acidity and catalytic activity, clearly TMPO adsorption can be used to verify and quantify framework incorporation of these heteroatoms. Specifically, the ^{31}P MAS NMR spectra of TMPO adsorbed on Ti-, Zr-, and Hf-Beta featured signals with similar widths and chemical shift ranges to those found for TMPO adsorbed on the tetrahedral framework sites in Sn-Beta (i.e., δ_{iso} ~ 60–50 ppm). In turn, analogous experiments using extra-framework HfO_2 in Si-Beta featured ^{31}P NMR chemical shifts similar to those observed with SnO_2 in Si-Beta (i.e., δ_{iso} < 45 ppm). These results are strong evidence that this method can corroborate if a Lewis acid heteroatom is tetrahedrally incorporated into the zeolite framework and opens exciting opportunities to further study these materials.

CONCLUSIONS

We have developed a method using ^{31}P MAS NMR spectroscopy and the probe molecule TMPO to characterize and quantify active sites in Lewis acid zeolites. This method can be utilized as a tool to quantify Lewis acid sites for zeolites with any heteroatom, providing access to information that is otherwise currently unavailable via NMR spectroscopy and other spectroscopic techniques. The TMPO method provides unprecedented information on active site speciation and concentration and allows us to assign certain ^{31}P chemical shifts to active sites for specific reactions. Importantly, we assigned the ^{31}P NMR resonances at δ_{iso} = 55.8 and 54.9 ppm to TMPO bound at the Sn environment in Sn-Beta zeolites responsible for glucose isomerization activity in water. The concentrations of these sites among the materials studied are consistent with the concentration of "open" sites that have previously been shown to be the active sites for this reaction. For aldol condensation, we have shown that the activity corresponds to a different type of Sn configuration in Sn-Beta, which manifests in the ^{31}P NMR spectra at δ_{iso} = 58.6 ppm with double titrations at δ_{iso} = 59.9 and 57.2 ppm. Overall, this method could be used to analyze any Lewis acid zeolite for any of the reactions that they catalyze to determine which sites are responsible for catalytic activity. This research elucidates structure–function relationships in Lewis acid zeolites, enabling catalyst improvement through rational design.

METHODS

Zeolites were synthesized according to reported protocols[2] and characterized by PXRD, N_2 adsorption/desorption, DRUV, SEM, and ICP-MS. TMPO dosing was conducted on freshly calcined zeolite samples that were degassed overnight under dynamic vacuum at 573 K to remove any adsorbed water. Samples were thereafter handled under dry nitrogen conditions. A DCM solution containing a known amount of TMPO was added to the sample tube with the zeolite and stirred overnight at room temperature. Finally, DCM was removed via heating to 353 K under a vacuum. For ^{31}P and ^{119}Sn MAS NMR analysis, samples dosed with TMPO were packed under an inert atmosphere into zirconia MAS NMR rotors with gastight caps. A Gaussian deconvolution method was used to analyze the quantitative ^{31}P MAS NMR spectra, and the % integrated ^{31}P peak area normalized by Sn content was calculated using the following formula: (mol site)/(mol total Sn) = (mol P/g-catalyst from ICP-MS) × (% peak area for specified site)/(mol Sn/g-catalyst from ICP-MS). Packed bed flow reactions were conducted in a tubular stainless steel reactor under differential conditions. Detailed methods and procedures can be found in the Supporting Information. No unexpected or unusually high safety hazards were encountered during this work.

ASSOCIATED CONTENT

Supporting Information

The Supporting Information is available free of charge on the ACS Publications website at DOI: 10.1021/acscatal.7b03533.

Experimental procedures including synthesis protocols, catalyst characterization methods, TMPO doing procedures, NMR methods, and reaction procedures; supplemental data and figures for catalyst characterization, NMR, reactivity, and titration (PDF)

AUTHOR INFORMATION

Corresponding Authors

*E-mail: vladimir.michaelis@ualberta.ca. Webpage: http://michaelis.chem.ualberta.ca..

*E-mail: yroman@mit.edu. Webpage: http://www.romangroup.mit.edu.

ORCID

Jennifer D. Lewis: 0000-0002-1874-9840

Vladimir K. Michaelis: 0000-0002-6708-7660

Yuriy Román-Leshkov: 0000-0002-0025-4233

Present Address

§Bernal Institute, University of Limerick, Limerick, Republic of Ireland V94 T9PX.

Notes

The authors declare no competing financial interest.

DOI: 10.1021/acscatal.7b03533
ACS Catal. 2018, 8, 3076–3086

■ ACKNOWLEDGMENTS

This work was supported by the U.S. Department of Energy, Office of Basic Energy Sciences under award No. DE-SC0016214. V.K.M. acknowledges the University of Alberta, Natural Sciences and Engineering Research Council (NSERC) of Canada Discovery Grant Program as well as NSERC CREATE and Deutsche Forschungsgemeinschaft DFG (IRTG2022) for Alberta/Technical University of Munich International Graduate School for Hybrid Functional Materials (ATUMS). J.D.L. was partially supported by the National Science Foundation Graduate Research Fellowship under grant no. 122374. Any opinion, findings, and conclusions or recommendations expressed in this material are those of the authors(s) and do not necessarily reflect the views of the National Science Foundation. M.H. was partially supported by a Queen Elizabeth II Fellowship. We thank M. Orella for taking SEM images. We thank Dr. V. Terskikh for acquiring some ^{119}Sn NMR spectra at the Canadian National Ultrahigh-Field NMR Facility for Solids (http://nmr900.ca).

■ REFERENCES

(1) Blasco, T.; Camblor, M.; Corma, A.; Esteve, P.; Guil, J.; Martinez, A.; Perdigon-Melon, J.; Valencia, S. Direct synthesis and characterization of hydrophobic aluminum-free Ti-beta zeolite. *J. Phys. Chem. B* **1998**, *102*, 75−88.

(2) Corma, A.; Nemeth, L. T.; Renz, M.; Valencia, S. Sn-zeolite beta as a heterogeneous chemoselective catalyst for Baeyer-Villiger oxidations. *Nature* **2001**, *412*, 423−425.

(3) Ennaert, T.; Van Aelst, J.; Dijkmans, J.; De Clercq, R.; Schutyser, W.; Dusselier, M.; Verboekend, D.; Sels, B. F. Potential and challenges of zeolite chemistry in the catalytic conversion of biomass. *Chem. Soc. Rev.* **2016**, *45*, 584−611.

(4) Moliner, M. State of the art of Lewis acid-containing zeolites: lessons from fine chemistry to new biomass transformation processes. *Dalton T.* **2014**, *43*, 4197−4208.

(5) Román-Leshkov, Y.; Davis, M. E. Activation of Carbonyl-Containing Molecules with Solid Lewis Acids in Aqueous Media. *ACS Catal.* **2011**, *1*, 1566−1580.

(6) Corma, A. From microporous to mesoporous molecular sieve materials and their use in catalysis. *Chem. Rev.* **1997**, *97*, 2373−2420.

(7) Holm, M. S.; Saravanamurugan, S.; Taarning, E. Conversion of Sugars to Lactic Acid Derivatives Using Heterogeneous Zeotype Catalysts. *Science* **2010**, *328*, 602−605.

(8) Luo, H. Y.; Bui, L.; Gunther, W. R.; Min, E.; Román-Leshkov, Y. Synthesis and Catalytic Activity of Sn-MFI Nanosheets for the Baeyer−Villiger Oxidation of Cyclic Ketones. *ACS Catal.* **2012**, *2*, 2695−2699.

(9) Bui, L.; Luo, H.; Gunther, W. R.; Román-Leshkov, Y. Domino reaction catalyzed by zeolites with Bronsted and Lewis acid sites for the production of gamma-valerolactone from furfural. *Angew. Chem., Int. Ed.* **2013**, *52*, 8022−8025.

(10) Corma, A.; Domine, M. E.; Nemeth, L.; Valencia, S. Al-Free Sn-Beta Zeolite as a Catalyst for the Selective Reduction of Carbonyl Compounds (Meerwein−Ponndorf−Verley Reaction). *J. Am. Chem. Soc.* **2002**, *124*, 3194−3195.

(11) Gunther, W. R.; Duong, Q.; Román-Leshkov, Y. Catalytic consequences of borate complexation and pH on the epimerization of l-arabinose to l-ribose in water catalyzed by Sn-Beta zeolite with borate salts. *J. Mol. Catal. A: Chem.* **2013**, *379*, 294−302.

(12) Luo, H. Y.; Lewis, J. D.; Román-Leshkov, Y. Lewis acid zeolites for biomass conversion: Perspectives and challenges on reactivity, synthesis, and stability. *Annu. Rev. Chem. Biomol. Eng.* **2016**, *7*, 663−692.

(13) Dapsens, P. Y.; Mondelli, C.; Perez-Ramirez, J. Design of Lewis-acid centres in zeolitic matrices for the conversion of renewables. *Chem. Soc. Rev.* **2015**, *44*, 7025−7043.

(14) Yakimov, A. V.; Kolyagin, Y. G.; Tolborg, S.; Vennestrøm, P. N.; Ivanova, I. I. ^{119}Sn MAS NMR Study of the Interaction of Probe Molecules with Sn-BEA: The Origin of Penta-and Hexacoordinated Tin Formation. *J. Phys. Chem. C* **2016**, *120*, 28083−28092.

(15) Gunther, W. R.; Michaelis, V. K.; Caporini, M. A.; Griffin, R. G.; Román-Leshkov, Y. Dynamic nuclear polarization NMR enables the analysis of Sn-Beta zeolite prepared with natural abundance ^{119}Sn precursors. *J. Am. Chem. Soc.* **2014**, *136*, 6219−6222.

(16) Wolf, P.; Valla, M.; Rossini, A. J.; Comas-Vives, A.; Núñez-Zarur, F.; Malaman, B.; Lesage, A.; Emsley, L.; Copéret, C.; Hermans, I. NMR Signatures of the Active Sites in Sn-β Zeolite. *Angew. Chem.* **2014**, *126*, 10343−10347.

(17) Copéret, C.; Liao, W.-C.; Gordon, C. P.; Ong, T.-C. Active Sites in Supported Single-Site Catalysts: An NMR Perspective. *J. Am. Chem. Soc.* **2017**, *139*, 10588−10596.

(18) Kolyagin, Y. G.; Yakimov, A. V.; Tolborg, S.; Vennestrøm, P. N.; Ivanova, I. I. Application of ^{119}Sn CPMG MAS NMR for Fast Characterization of Sn Sites in Zeolites with Natural ^{119}Sn Isotope Abundance. *J. Phys. Chem. Lett.* **2016**, *7*, 1249−1253.

(19) Boronat, M.; Concepcion, P.; Corma, A.; Renz, M.; Valencia, S. Determination of the catalytically active oxidation Lewis acid sites in Sn-beta zeolites, and their optimization by the combination of theoretical and experimental studies. *J. Catal.* **2005**, *234*, 111−118.

(20) Harris, J. W.; Cordon, M. J.; Di Iorio, J. R.; Vega-Vila, J. C.; Ribeiro, F. H.; Gounder, R. Titration and quantification of open and closed Lewis acid sites in Sn-Beta zeolites that catalyze glucose isomerization. *J. Catal.* **2016**, *335*, 141−154.

(21) Wang, Y.; Lewis, J. D.; Román-Leshkov, Y. Synthesis of Itaconic Acid Ester Analogues via Self-Aldol Condensation of Ethyl Pyruvate Catalyzed by Hafnium BEA Zeolites. *ACS Catal.* **2016**, *6*, 2739−2744.

(22) Sushkevich, V. L.; Vimont, A.; Travert, A.; Ivanova, I. I. Spectroscopic Evidence for Open and Closed Lewis Acid Sites in ZrBEA Zeolites. *J. Phys. Chem. C* **2015**, *119*, 17633−17639.

(23) Sushkevich, V. L.; Palagin, D.; Ivanova, I. I. With Open Arms: Open Sites of ZrBEA Zeolite Facilitate Selective Synthesis of Butadiene from Ethanol. *ACS Catal.* **2015**, *5*, 4833−4836.

(24) Gunther, W. R.; Michaelis, V. K.; Griffin, R. G.; Román-Leshkov, Y. Interrogating the Lewis acidity of metal sites in beta zeolites with ^{15}N pyridine adsorption coupled with MAS NMR spectroscopy. *J. Phys. Chem. C* **2016**, *120*, 28533−28544.

(25) Harris, J. W.; Liao, W.-C.; Di Iorio, J. R.; Henry, A. M.; Ong, T.-C.; Comas-Vives, A.; Copéret, C.; Gounder, R. Molecular Structure and Confining Environment of Sn Sites in Single-Site Chabazite Zeolites. *Chem. Mater.* **2017**, *29*, 8824−8837.

(26) Zheng, A.; Liu, S.-B.; Deng, F. ^{31}P NMR Chemical Shifts of Phosphorus Probes as Reliable and Practical Acidity Scales for Solid and Liquid Catalysts. *Chem. Rev.* **2017**, *117*, 12475−12531.

(27) Seo, Y.; Cho, K.; Jung, Y.; Ryoo, R. Characterization of the surface acidity of MFI zeolite nanosheets by ^{31}P NMR of adsorbed phosphine oxides and catalytic cracking of decalin. *ACS Catal.* **2013**, *3*, 713−720.

(28) Zheng, A.; Huang, S. J.; Liu, S. B.; Deng, F. Acid properties of solid acid catalysts characterized by solid-state ^{31}P NMR of adsorbed phosphorous probe molecules. *Phys. Chem. Chem. Phys.* **2011**, *13*, 14889−14901.

(29) Rakiewicz, E. F.; Peters, A. W.; Wormsbecher, R. F.; Sutovich, K. J.; Mueller, K. T. Characterization of acid sites in zeolitic and other inorganic systems using solid-state ^{31}P NMR of the probe molecule trimethylphosphine oxide. *J. Phys. Chem. B* **1998**, *102*, 2890−2896.

(30) Chu, Y.; Yu, Z.; Zheng, A.; Fang, H.; Zhang, H.; Huang, S.-J.; Liu, S.-B.; Deng, F. Acidic Strengths of Brønsted and Lewis Acid Sites in Solid Acids Scaled by ^{31}P NMR Chemical Shifts of Adsorbed Trimethylphosphine. *J. Phys. Chem. C* **2011**, *115*, 7660−7667.

(31) Zhuang, J.; Yan, Z.; Liu, X.; Liu, X.; Han, X.; Bao, X.; Mueller, U. NMR study on the acidity of TS-1 zeolite. *Catal. Lett.* **2002**, *83*, 87−91.

(32) Zhuang, J.; Ma, D.; Yan, Z.; Deng, F.; Liu, X.; Han, X.; Bao, X.; Liu, X. W.; Guo, X.; Wang, X. Solid-state MAS NMR detection of the

DOI: 10.1021/acscatal.7b03533
ACS Catal. 2018, 8, 3076−3086

oxidation center in TS-1 zeolite by in situ probe reaction. *J. Catal.* **2004**, *221*, 670−673.
(33) Zhang, W.; Xu, S.; Han, X.; Bao, X. In situ solid-state NMR for heterogeneous catalysis: a joint experimental and theoretical approach. *Chem. Soc. Rev.* **2012**, *41*, 192−210.
(34) Zhao, Q.; Chen, W.-H.; Huang, S.-J.; Wu, Y.-C.; Lee, H.-K.; Liu, S.-B. Discernment and quantification of internal and external acid sites on zeolites. *J. Phys. Chem. B* **2002**, *106*, 4462−4469.
(35) Hwang, S.-J.; Gounder, R.; Bhawe, Y.; Orazov, M.; Bermejo-Deval, R.; Davis, M. E. Solid State NMR Characterization of Sn-Beta Zeolites that Catalyze Glucose Isomerization and Epimerization. *Top. Catal.* **2015**, *58*, 435−440.
(36) Chen, H. S.; Wang, A.; Sorek, H.; Lewis, J. D.; Román-Leshkov, Y.; Bell, A. Production of Hydroxyl−rich Acids from Xylose and Glucose Using Sn-BEA Zeolite. *ChemistrySelect* **2016**, *1*, 4167−4172.
(37) Yang, G.; Zhou, L.; Han, X. Lewis and Brönsted acidic sites in M 4+-doped zeolites (M= Ti, Zr, Ge, Sn, Pb) as well as interactions with probe molecules: A DFT study. *J. Mol. Catal. A: Chem.* **2012**, *363*, 371−379.
(38) Yoder, C. H.; Margolis, L. A.; Horne, J. M. A Tin-119 NMR investigation of phosphine and phosphine oxide adducts of organotin chlorides. *J. Organomet. Chem.* **2001**, *633*, 33−38.
(39) Michaelis, V. K.; Aguiar, P. M.; Kroeker, S. Probing alkali coordination environments in alkali borate glasses by multinuclear magnetic resonance. *J. Non-Cryst. Solids* **2007**, *353*, 2582−2590.
(40) Clayden, N. J.; Dobson, C. M.; Fern, A. High-resolution solid-state Tin-119 nuclear magnetic resonance spectroscopy of ternary tin oxides. *J. Chem. Soc., Dalton Trans.* **1989**, 843−847.
(41) Wolf, P.; Liao, W.-C.; Ong, T.-C.; Valla, M.; Harris, J. W.; Gounder, R.; van der Graaff, W. N. P.; Pidko, E. A.; Hensen, E. J. M.; Ferrini, P.; Dijkmans, J.; Sels, B.; Hermans, I.; Copéret, C. Identifying Sn Site Heterogeneities Prevalent Among Sn-Beta Zeolites. *Helv. Chim. Acta* **2016**, *99*, 916−927.
(42) Tolborg, S.; Katerinopoulou, A.; Falcone, D. D.; Sádaba, I.; Osmundsen, C. M.; Davis, R.; Taarning, E.; Fristrup, P.; Holm, M. S. Incorporation of tin affects crystallization, morphology, and crystal composition of Sn-Beta. *J. Mater. Chem. A* **2014**, *2*, 20252−20262.
(43) Bermejo-Deval, R.; Gounder, R.; Davis, M. E. Framework and Extraframework Tin Sites in Zeolite Beta React Glucose Differently. *ACS Catal.* **2012**, *2*, 2705−2713.
(44) Román-Leshkov, Y.; Moliner, M.; Labinger, J. A.; Davis, M. E. Mechanism of glucose isomerization using a solid Lewis acid catalyst in water. *Angew. Chem., Int. Ed.* **2010**, *49*, 8954−8957.
(45) Lewis, J. D.; Van de Vyver, S.; Román-Leshkov, Y. Acid-Base Pairs in Lewis Acidic Zeolites Promote Direct Aldol Reactions by Soft Enolization. *Angew. Chem., Int. Ed.* **2015**, *54*, 9835−9838.
(46) Dijkmans, J.; Demol, J.; Houthoofd, K.; Huang, S.; Pontikes, Y.; Sels, B. Post-synthesis Snβ: An exploration of synthesis parameters and catalysis. *J. Catal.* **2015**, *330*, 545−557.
(47) Bermejo-Deval, R.; Assary, R. S.; Nikolla, E.; Moliner, M.; Román-Leshkov, Y.; Hwang, S. J.; Palsdottir, A.; Silverman, D.; Lobo, R. F.; Curtiss, L. A.; Davis, M. E. Metalloenzyme-like catalyzed isomerizations of sugars by Lewis acid zeolites. *Proc. Natl. Acad. Sci. U. S. A.* **2012**, *109*, 9727−9732.
(48) Bermejo-Deval, R.; Orazov, M.; Gounder, R.; Hwang, S. J.; Davis, M. E. Active Sites in Sn-Beta for Glucose Isomerization to Fructose and Epimerization to Mannose. *ACS Catal.* **2014**, *4*, 2288−2297.
(49) Boronat, M.; Corma, A.; Renz, M. Mechanism of the Meerwein-Ponndorf-Verley-Oppenauer (MPVO) redox equilibrium on Sn- and Zr-beta zeolite catalysts. *J. Phys. Chem. B* **2006**, *110*, 21168−21174.
(50) Wolf, P.; Valla, M.; Nunez-Zarur, F.; Comas-Vives, A.; Rossini, A. J.; Firth, C.; Kallas, H.; Lesage, A.; Emsley, L.; Copéret, C.; Hermans, I. Correlating synthetic methods, morphology, atomic-level structure, and catalytic activity of Sn-β catalysts. *ACS Catal.* **2016**, *6*, 4047−4063.
(51) Li, Y. P.; Head-Gordon, M.; Bell, A. T. Analysis of the Reaction Mechanism and Catalytic Activity of Metal-Substituted Beta Zeolite for the Isomerization of Glucose to Fructose. *ACS Catal.* **2014**, *4*, 1537−1545.
(52) Shetty, S.; Pal, S.; Kanhere, D. G.; Goursot, A. Structural, Electronic, and Bonding Properties of Zeolite Sn-Beta: A Periodic Density Functional Theory Study. *Chem. - Eur. J.* **2006**, *12*, 518−523.
(53) Yang, G.; Pidko, E. A.; Hensen, E. J. Structure, Stability, and Lewis Acidity of Mono and Double Ti, Zr, and Sn Framework Substitutions in BEA Zeolites: A Periodic Density Functional Theory Study. *J. Phys. Chem. C* **2013**, *117*, 3976−3986.
(54) Sastre, G.; Corma, A. Relation between structure and Lewis acidity of Ti-Beta and TS-1 zeolites: A quantum-chemical study. *Chem. Phys. Lett.* **1999**, *302*, 447−453.
(55) Josephson, T. R.; Jenness, G. R.; Vlachos, D. G.; Caratzoulas, S. Distribution of open sites in Sn-Beta zeolite. *Microporous Mesoporous Mater.* **2017**, *245*, 45−50.
(56) Boronat, M.; Corma, A.; Renz, M.; Viruela, P. M. Predicting the activity of single isolated Lewis acid sites in solid catalysts. *Chem. - Eur. J.* **2006**, *12*, 7067−7077.
(57) Gounder, R.; Davis, M. E. Monosaccharide and disaccharide isomerization over Lewis acid sites in hydrophobic and hydrophilic molecular sieves. *J. Catal.* **2013**, *308*, 176−188.
(58) Luo, H. Y.; Consoli, D. F.; Gunther, W. R.; Román-Leshkov, Y. Investigation of the reaction kinetics of isolated Lewis acid sites in Beta zeolites for the Meerwein-Ponndorf-Verley reduction of methyl levulinate to gamma-valerolactone. *J. Catal.* **2014**, *320*, 198−207.
(59) Bregante, D. T.; Flaherty, D. W. Periodic Trends in Olefin Epoxidation over Group IV and V Framework-Substituted Zeolite Catalysts: A Kinetic and Spectroscopic Study. *J. Am. Chem. Soc.* **2017**, *139*, 6888−6898.

DOI: 10.1021/acscatal.7b03533
ACS Catal. 2018, 8, 3076−3086